Laser and Particle Beams (2012), *30*, 103–109.

doi:10.1017/S0263034611000735

Effects of long rarefied plasma on fast electron generation for FIREX-I targets

H. SAKAGAMI,[1] A. SUNAHARA,[2] T. JOHZAKI,[2] AND H. NAGATOMO[3]

[1]Fundamental Physics Simulation Division, National Institute for Fusion Science, Toki, Japan
[2]Institute for Laser Technology, Suita, Japan
[3]Institute of Laser Engineering, Osaka University, Suita, Japan

(RECEIVED 3 June 2011; ACCEPTED 29 October 2011)

Abstract

Long-scale preformed plasmas are generated inside the cone by the pre-pulse of the heating laser in the cone-guided fast ignition scheme and it is found that coupling efficiency from the heating laser to fast electrons especially suitable for core heating is drastically reduced by the preformed plasmas. To mitigate this serious problem, an extremely thin film is suggested to cover the entrance of the cone. This method, however, introduces long rarefied plasmas around the entrance of the cone and the main pulse must propagate through these plasmas. Therefore, fast electron characteristics produced by the main pulse could be affected, and effects of long rarefied plasmas on fast electron generation are investigated. It is found that the electron beam intensity becomes larger than that without the rarefied plasma, but the energy coupling rate from the heating laser to the core decreases due to lack of appropriate electrons for core heating. To achieve less than 10% degradation of the core electron temperature, the thin film must be expanded by irradiation of the pre-pulse so that the length and the density of rarefied plasmas become less than 500 μm and one-tenth of the critical density. A thickness of the thin film can be determined by these criteria and the intensity of the pre-pulse.

Keywords: Cone-guided target; Fast electron; Fast ignition; Integrated simulation

1. INTRODUCTION

The FIREX-I project (Azechi & FIREX Project, 2008) aims to demonstrate that the imploded core could be heated up to 5 keV, and incorporated experiments for FIREX-I, in which heating is combined with implosion, have started at Institute of Laser Engineering, Osaka University. Efficient heating mechanisms and achievement of such high temperature have not been, however, clarified yet, and we have been promoting the fast ignition integrated interconnecting code (FI^3) project to boldly explore fast ignition frontiers (Sakagami & Mima, 2004; Nakamura *et al.*, 2006, 2008; Sakagami, *et al.*, 2006, 2009; Johzaki, *et al.*, 2007, 2010). First series of the incorporated experiments was performed in 2009, and only 30-fold enhancement in neutron yield, which was about 1/30 smaller than that in 2002 experiments (Kodama *et al.*, 2002), was achieved and a lower energy coupling rate from the heating laser to the imploded core was expected (Mima *et al.*, 2010). According to two-dimensional core heating simulations where a uniform core heating rate was assumed, the energy coupling rate from the heating laser to the compressed core could be estimated around 20% in 2002 experiments, but less than 5% in 2009 experiments (Johzaki, *et al.*, 2011). An unavoidable pre-pulse of the heating laser generates long-scale low-density plasmas (preformed plasmas) inside the cone. A main pulse of the heating laser has to interact with these long-scale preformed plasmas and it results in increasing the distance from the generation point of fast electrons to the core, and generating too energetic fast electrons (Kemp *et al.*, 2009). In turn, low energy fast electrons especially suitable for core heating decease and it leads to low coupling efficiency.

To mitigate preformed plasma problems, the entrance of the cone is suggested to be covered with an extremely thin film. As the pre-pulse could be interrupted and absorbed by this film, the cone wall cannot be irradiated with the pre-pulse and the preformed plasmas are not produced. But the region around the entrance of the cone is filled with rarefied plasmas, which are the residue of expanding thin film plasmas. Thus, the main pulse of the heating laser must propagate through very long (>500 μm) rarefied ($\ll n_{cr}$) plasmas,

Address correspondence and reprint requests to: H. Sakagami, Fundamental Physics Simulation Division, National Institute for Fusion Science, 322-6 Oroshi-cho, Toki 509-5292, Japan. E-mail: sakagami.hitoshi@nifs.ac.jp

where n_{cr} is the critical density. However, there has been few research using such long rarefied plasmas, and we have investigated effects of long rarefied plasmas on core heating with the use of FI^3, which consists of two radiation-hydro codes, PINOCO (Nagatomo *et al.*, 2002) for implosion and STAR-2D (Sunahara *et al.*, 2008) for pre-plasma formation, two particle-in-cell codes, FISCOF (Sakagami & Mima, 2002) and ASCENT (Cai *et al.*, 2009) for relativistic laser-plasma interaction and one Fokker Planck-hydro code FIBMET (Johzaki, *et al.*, 2006) for core heating process.

2. SUPPRESSION OF PREFORMED PLASMA

2.1. Pre-Pulse and Preformed Plasma

The plasma profile inside the cone was measured by X-ray pinhole images in 2009 experiments (Mima *et al.*, 2010). The time-integrated X-ray image shows a wide bright area at ~100 μm away from the cone tip. It means that the heating laser is absorbed far away from the cone tip even though it is focused at the center of the cone tip, and indicates that the inside of the cone is filled with preformed plasmas, which are generated by the pre-pulse. To estimate the pre-pulse level, we compared STAR-2D simulation results with experimental data for planar targets (Sunahara *et al.*, 2011). When the laser intensity in the simulation is 10^{13} W/cm^2, the density scale length of the preformed plasma is measured as 100 μm and the blow off speed of ablated plasmas as 1×10^7 cm/s at 1 ns. These values are in good agreement with experimental observations, and we can conclude that the cone is illuminated by the pre-pulse of the heating laser with 10^{13} W/cm^2 intensity and 1 ns duration before it is irradiated by the main pulse. The corresponding pre-pulse energy is estimated to be 130 mJ. For the next step, we also simulated the pre-plasma formation inside the cone with STAR-2D (Sunahara *et al.*, 2011). The temporal profile of the laser is flattop with 1 ns duration, and the wavelength and the spot diameter are set to 1.06 μm and 40 μm (Gaussian FWHM), respectively. The tip diameter of the cone is 30 μm. Preformed plasma profiles are shown in Figure 1 for different intensities (1×10^{11}, 1×10^{12}, and 1×10^{13} W/cm^2) and different open angles (30°, 45°, and 60°) after 1 ns irradiation. For the pre-pulse intensity estimated above (10^{13} W/cm^2) and the open angle in 2009 experiments (30° or 45°), the preformed plasma expands to the inner space of the cone up to 300 μm away from the cone tip. As the cone with the larger open angle has the larger volume to be filled, the density scale length of the preformed plasma is reduced when the open angle of the cone increases. While the critical density ($n_{cr} = 10^{21}$ cm^{-3} for 1.06 μm laser) point is still close to the cone tip, underdense plasmas with long-scale length exist inside the cone and the main pulse of the heating laser must interact with these plasmas.

To evaluate preformed plasma effects inside the cone, we carried out ASCENT-2D simulations (Johzaki, *et al.*, 2011). The Au cone plasma (Z = 40, $100n_{cr}$, 30° open angle, 12 μm tip inner width, 5 μm tip thickness and 8 μm side wall thickness) is surrounded by the imploded CD plasma ($Z = 3.5$ and $50n_{cr}$). As the case without preformed plasmas, surface plasmas with the short scale length (1 μm) from $100n_{cr}$ to $0.1n_{cr}$ are introduced in front of the cone tip. According to preformed plasma parameters in Figure 1 simulated by STAR-2D, the scale length of plasmas ablated by the pre-pulse is very short in overdense region and relatively longer in underdense region. Thus, preformed plasmas with the scale length 10 μm are attached from $5n_{cr}$ point in addition to surface plasmas for the case with preformed plasmas. The cone is irradiated by the *p*-polarized main pulse of the heating laser with 1.06 μm wavelengths, 3×10^{19} W/cm^2 intensity and 16.5 μm spot diameter (Gaussian FWHM). The laser rises to its peak within 33 fs. Fast electron energy densities at 1 ps are shown in Figure 2 for both (a) without and (b) with preformed plasmas. For the case without preformed plasmas, the central part of the main pulse directly hits the tip of the cone, and the surrounding parts are reflected at the sidewall of the cone and headed to the tip. Thus, most of fast electrons are generated at the tip. On the other hand, fast electrons are mainly generated in the underdense

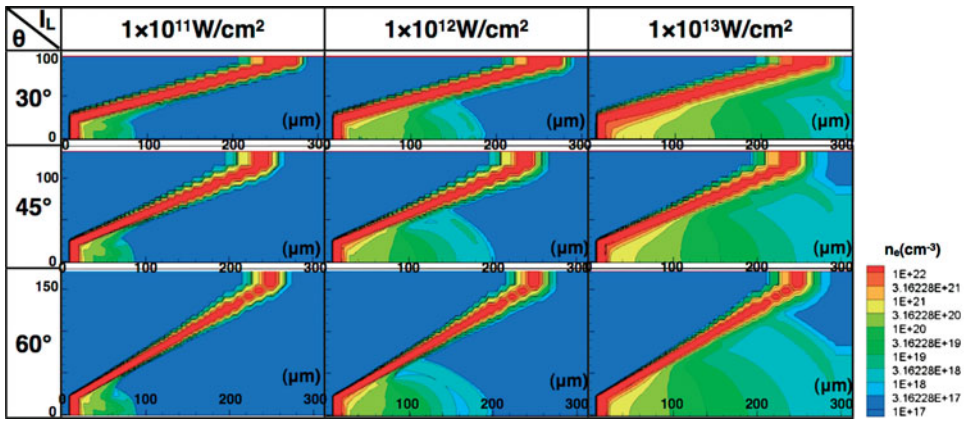

Fig. 1. (Color online) Preformed plasma profiles for different intensities of the pre-pulse (1×10^{11}, 1×10^{12} or 1×10^{13} W/cm^2) and different open angles of the cone (30°, 45°, or 60°) after 1 ns irradiation.

https://doi.org/10.1017/S0263034611000735 Published online by Cambridge University Press

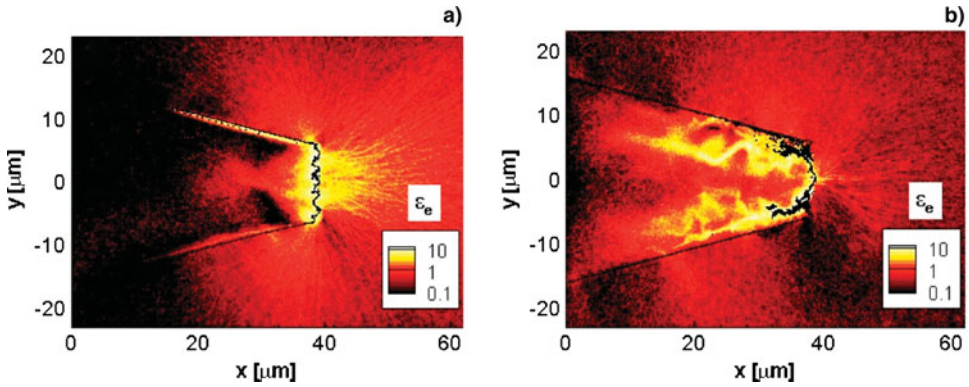

Fig. 2. (Color online) Fast electron energy densities at 1 ps for (**a**) without and (**b**) with preformed plasmas. Energy density is normalized by $m_e \cdot c^2 \cdot n_{cr}$, where m_e and c are electron rest mass and speed of light, respectively.

preformed plasma region and their energy is much higher than that without the preformed plasma case.

Energy coupling rates from the heating laser to all fast electrons or to low-energy (<10 MeV) fast electrons observed at the cone tip (15 μm width) are summarized in Table 1. The energy coupling rate is reduced in the case with preformed plasmas. This reduction, however, is much significant, namely about 1/4 for the case to low-energy fast electrons, which are more suitable for heating the core. In addition, fewer fast electrons can reach the core than those without preformed plasmas as the preformed plasma makes the distance from the generation point of fast electrons to the core longer. Therefore, coupling efficiency from the heating laser to the core is drastically degraded by the preformed plasma and it is indispensable to reduce the pre-pulse level as small as possible for efficient core heating. According to STAR-2D simulations, preformed plasmas are much localized around the cone tip when the pre-pulse intensity is 1×10^{11} W/cm^2 (see Fig. 1), and we can expect very little effect of the preformed plasma. This means that we must reduce the pre-pulse level to about 1/100 compared with the current status.

From an additional point of view, the Au cone tip causes the degradation of the energy coupling due to collisional and resistive drags during the transport of fast electrons in the cone tip. Therefore CH is proposed as an alternative material of the cone tip to reduce collisional defects and it is found that in comparison with the Au cone tip, a twice higher rise in temperature of the compressed CD core has been achieved with the CH cone tip (Johzaki *et al.*, 2009). The CH cone tip has another good feature that the preformed plasma would be smaller than that with the Au cone tip due to low-*Z* materiality. Thus, using the CH cone instead of the Au cone could also improve this severe problem to a certain extent, but it's beyond this paper.

Table 1. *Energy coupling rates from laser to fast electrons*

	energy coupling rate [%]	
	to all	to low-energy (E < 10 MeV)
without preformed plasma	48	39
with preformed plasma	36	11

2.2. Thin Film Absorber

An amplified optical parametric fluorescence quencher (Kondo *et al.*, 2006) or a saturable absorber can be used to suppress the pre-pulse level. It is, however, still a technical challenge to maintain the pre-pulse intensity below 1×10^{11} W/cm^2. The other method to mitigate the pre-pulse problem, the entrance of the cone is suggested to be covered with an extremely thin film. The pre-pulse could be interrupted and absorbed by this film, and the cone wall cannot be irradiated by the pre-pulse and long-scale preformed plasmas are not produced (Kinoshita *et al.*, 2004; Mima *et al.*, 2010). Before the cone is irradiated by the main pulse, this film should be ionized by the pre-pulse and must diffuse to quite low density not to disturb the main pulse propagation. As the pulse duration of the pre-pulse is the order of nano second, plasmas are expected to expand much below the critical density.

To evaluate remnant plasmas of the thin film, we performed STAR-2D simulations (Sunahara *et al.*, 2011). As the thin film is placed at the entrance of the cone 1 mm away from the cone tip, the irradiation intensity and the spot size are lower and larger than those at the focus point. So we assume the pre-pulse of 3×10^{11} W/cm^2 intensity, 100 μm spot diameter (Gaussian FWHM) and flattop temporal profile. The thin film, which is made from CH and 0.1 μm thickness is irradiated by this pre-pulse. Contour plots of the electron density are shown in Figure 3 at (a) 1.2 ns and (b) 1.8 ns. The electron density and the thickness of plasmas within the spot diameter along the laser axis become below 1/10 of the critical density and about 500 μm at 1.2 ns, or 1/30 and 800 μm at 1.8 ns, respectively.

https://doi.org/10.1017/S0263034611000735 Published online by Cambridge University Press

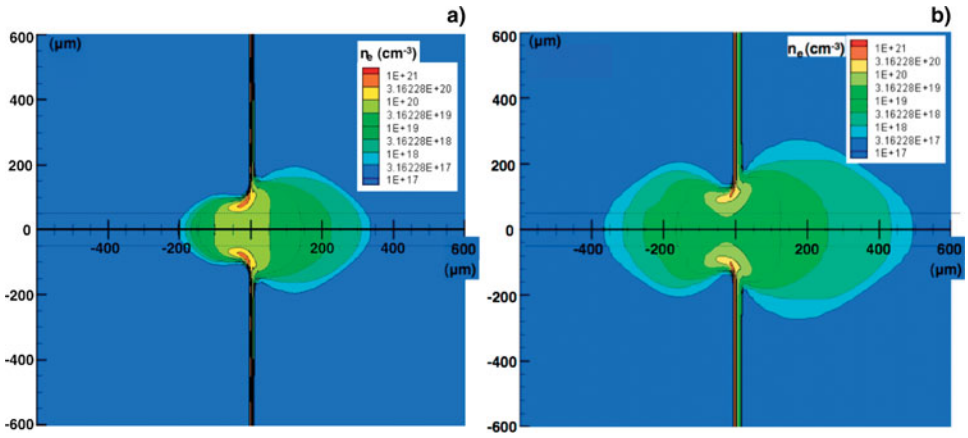

Fig. 3. (Color online) Electron density contour plots for remnant plasmas of the thin film at (**a**) 1.2 ns and (**b**) 1.8 ns.

Anyway, the main pulse must propagate through these very long rarefied plasmas.

3. LONG RAREFIED PLASMA

3.1. Fast Electron Characteristics

To investigate effects of the long rarefied plasma around the entrance of the cone on fast electron characteristics, laser-plasma interactions are computed by FISCOF-1D using a time step of 5×10^{-3} fs, a resolution of 250 cells per laser wavelength, up to 200 particles per cell for electrons or ions. The heating laser is set to $I_L = 10^{20}$ W/cm^2, $\lambda_L =$ 1.06 μm, $\tau_{FWHM} = 1$ ps Gaussian, and the Au ($A = 197$, $Z = 30$) cone tip is introduced as a 10 μm, $500n_{cr}$ flat profile plasma, which is followed by 20 μm long CD ($500n_{cr}$, $A = 7$, $Z = 3.5$) plasma. We put the CH foam plasma ($10n_{cr}$, $A =$ 6.5, $Z = 3.5$) with 50 μm thickness in front of the Au cone tip plasma to efficiently generate fast electrons (Sakagami *et al.*, 2009). We also put the H uniform plasma ($A = 1$, $Z = 1$, $L_{rare} = 150$ or 300 μm thickness) with different densities ($n_{rare} = 0.01n_{cr} \sim n_{cr}$) in front of the CH foam plasma as the long rarefied plasma. The proton-electron mass ratio is set to1836, and initial temperatures of electrons and ions in all plasmas are set to 10 and 0.3 keV, respectively. A fast electron beam is observed in CD plasma, 10 μm behind the Au-CD boundary. To ignore a circulation of fast electrons that are reflected by the sheath field at the right edge of the CD plasma, we introduce an artificial cooling region (7 μm long) at the rear of CD plasma, in which fast electrons are gradually cooled down to the initial temperature.

Time evolutions of fast electron beam intensity are shown in Figure 4 without rarefied plasmas and with rarefied plasmas of different densities (0.01, 0.05, 0.1, 0.5, and $1n_{cr}$) for (a) $L_{rare} = 150$ and (b) 300 μm. As the intensity of the heating laser is 10^{20} W/cm^2, the fast electron beam intensity of 10^{19} W/cm^2 means that the instantaneous energy coupling rate from the laser to fast electrons is 10%. Fast electron beam intensities are similar to those in the case without rarefied plasmas for $n_{rare} < 0.1n_{cr}$ with $L_{rare} = 150$ μm and $n_{rare} = 0.01n_{cr}$ with $L_{rare} = 300$ μm. On the other hand, fast electron beam intensities become larger than that without rarefied plasmas due to the large energy coupling rate from the laser to electrons for $n_{rare} > 0.5n_{cr}$ with $L_{rare} = 150$ μm and $n_{rare} > 0.05n_{cr}$ with $L_{rare} = 300$ μm. When the laser propagates through the plasma, a group velocity of light becomes slower as the density increases. So the leading edge of the fast electron beam delays more with the larger density of the rarefied plasma in the case of $n_{rare} > 0.5n_{cr}$ with $L_{rare} =$ 150 μm. The rarefied plasma with $L_{rare} = 300$ μm enhances this delay much more. Total fast electron fluences, which are calculated by time-integrating fast electron beam intensities, are shown in Figure 5 as a function of $\rho L\, n_{cr}$·μm for both

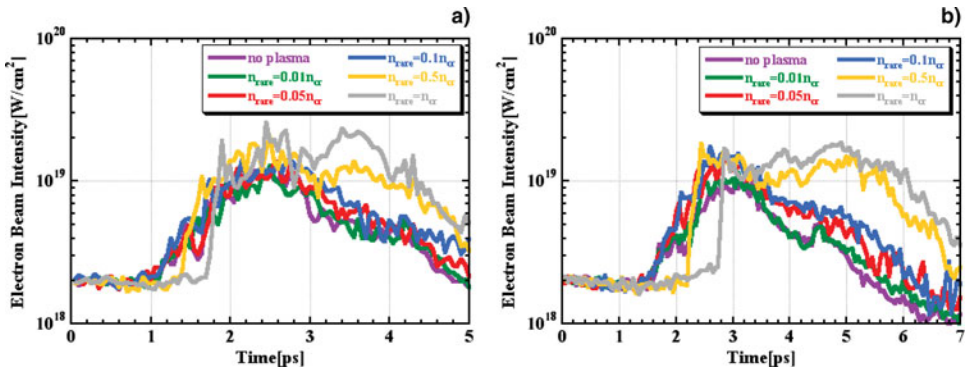

Fig. 4. (Color online) Time evolutions of fast electron beam intensity without rarefied plasmas (purple) and with rarefied plasmas of different densities, 0.01(green), 0.05(red), 0.1(blue), 0.5(yellow), and 1(gray) n_{cr} for (**a**) L_{rare}=150 and (**b**) 300 μm.

https://doi.org/10.1017/S0263034611000735 Published online by Cambridge University Press

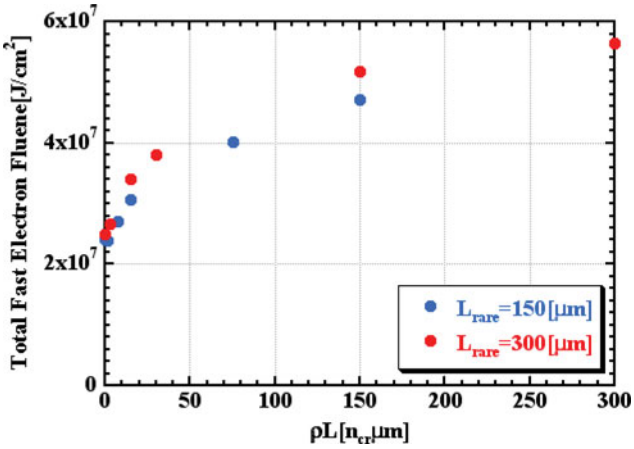

Fig. 5. (Color online) Total fast electron fluences as a function of ρL n_{cr}·μm for both L_{rare} = 150(blue) and 300(red) μm.

$L_{rare} = 150$ and 300 μm, where ρ and L are the rarefied plasma density and thickness, respectively. In the case without rarefied plasmas ($\rho L = 0$), fast electrons are mainly generated by interactions between the heating laser and the CH foam plasma, and the total fast electron fluence of about 2.4×10^7 J/cm^2 is obtained. If the rarefied plasma exists, the laser is absorbed within underdense plasmas and generates very energetic fast electrons. Thus, energy increment of fast electrons is roughly proportional to ρL due to absorption increment up to $\rho L = 150$ n_{cr}·μm. When ρL is 300 n_{cr}·μm, the energy increment tends to saturate because the laser intensity decreases before reaching the CH foam plasma due to large absorption. So less fast electrons are generated by interactions between the heating laser and the CH foam plasma.

Time averaged fast electron energy distributions are shown in Figure 6 without rarefied plasmas and with rarefied plasmas of different densities (0.01, 0.05, 0.1, 0.5, and $1n_{cr}$) for (a) $L_{rare} = 150$ and (b) 300 μm with wide energy range, and (c) $L_{rare} = 150$, and (d) 300 μm with narrow energy range. When the density of the rarefied plasma is less than $0.1n_{cr}$ for $L_{rare} = 150$ μm or $0.05n_{cr}$ for 300 μm, fast electron energy distributions are almost same as those in the case without rarefied plasmas. If the density is greater than $0.5n_{cr}$ for $L_{rare} = 150$ μm or $0.1n_{cr}$ for 300 μm, more laser energy is absorbed by the underdense rarefied plasma, and fast electrons with energies above 3 MeV are generated much more. They mainly contribute enhancement of the fast electron beam intensity (see Fig. 4), however, and these energetic fast electrons are not suitable for core heating at all. Fast electrons with energies less than 2 MeV are strongly reduced in the case of $n_{rare} = n_{cr}$ and $L_{rare} =$ 300 μm, because the heating laser is exhausted by the long rarefied plasma prior to reach the CH foam plasma and it can not generate many fast electrons with moderated energy from the CH foam plasma.

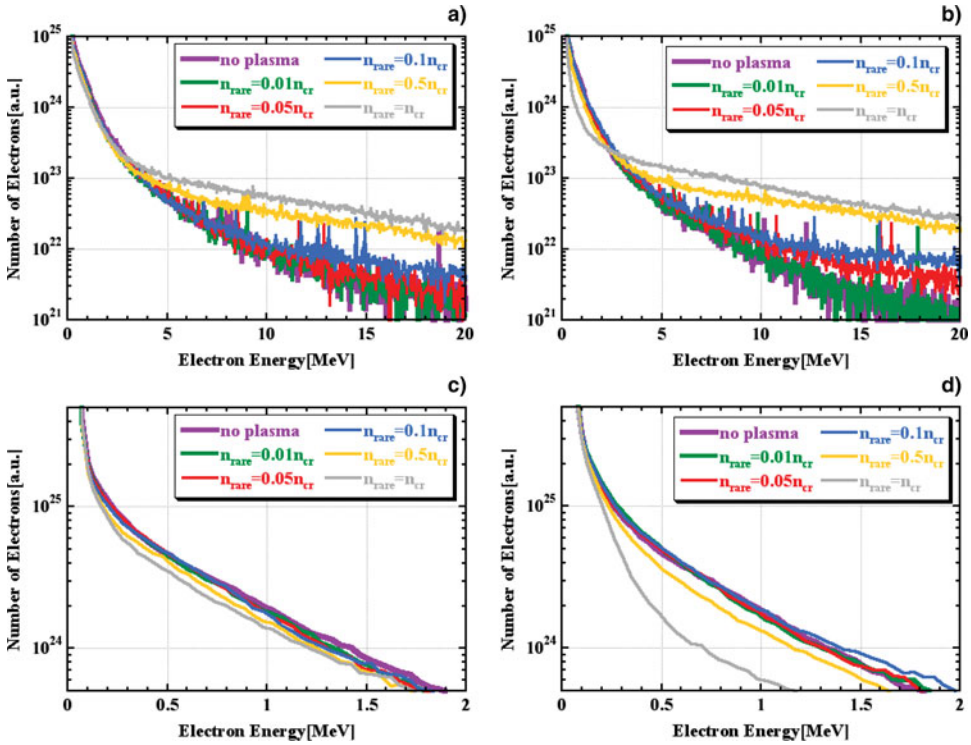

Fig. 6. (Color online) Time averaged fast electron energy distributions without rarefied plasmas and with rarefied plasmas of different densities (0.01, 0.05, 0.1, 0.5, and $1n_{cr}$) for (**a**) $L_{rare} = 150$ and (**b**) 300 μm with wide energy range, and (**c**) $L_{rare} = 150$ and (**d**) 300 μm with narrow energy range. Line colors of purple, green, red, blue, yellow and gray indicate 0 (without rarefied plasma), 0.01, 0.05, 0.1, 0.5, and $1n_{cr}$, respectively.

https://doi.org/10.1017/S0263034611000735 Published online by Cambridge University Press

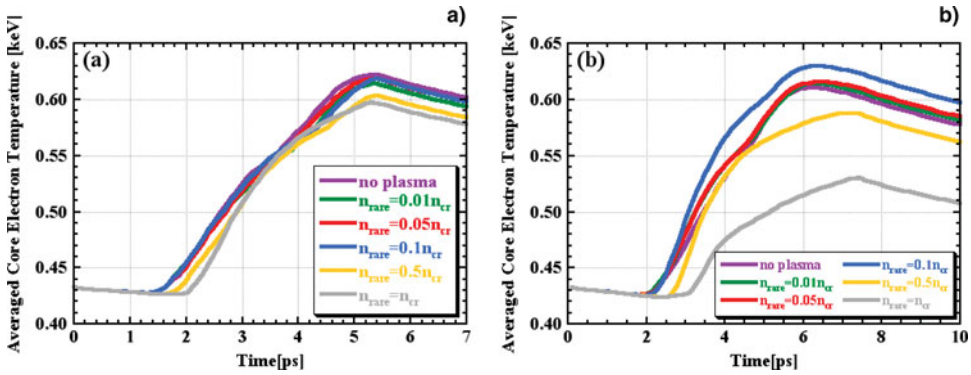

Fig. 7. (Color online) Time evolutions of averaged core electron temperature over the dense region ($\rho > 10$ g/cm^3) without rarefied plasmas (purple) and with rarefied plasmas of different densities, 0.01(green), 0.05(red), 0.1(blue), 0.5(yellow), and 1(gray) n_{cr} for (**a**) L_{rare} = 150 and (**b**) 300 μm.

3.2. Integrated Simulations for Core Heating

As core heating is greatly affected by not only the beam intensity but also the energy distribution of fast electrons, we have performed FI^3 integrated simulations to estimate core temperatures, assuming the same core parameters as in Johzaki *et al.* (2007). Observed fast electron profiles by FISCOF-1D in the previous section are used as the time-dependent momentum distributions of fast electrons for FIBMET-1D. Time evolutions of averaged core electron temperature computed by FIBMET-1D, which are averaged over the dense region ($\rho > 10$ g/cm^3), are shown in Figure 7 without rarefied plasmas and with rarefied plasmas of different densities (0.01, 0.05, 0.1, 0.5, and $1n_{cr}$) for (a) L_{rare} = 150 and (b) 300 μm. Maximum averaged core electron temperature is measured from Figure 7, and the increment from the initial temperature is calculated. Degradations of electron temperature increment against the case without rarefied plasmas are shown in Figure 8 as a function of ρL n_{cr}·μm for both L_{rare} = 150 and 300 μm. In the case of 150 μm thickness rarefied plasma, fast electrons that are suitable for core heating (< 2 MeV) are not affected so much by the rarefied plasma (see Fig. 6c), and time evolutions are similar to the case without rarefied plasmas. Thus, the maximum core electron temperature is only reduced by 15% even for the $n_{rare} = n_{cr}$ case. The electron temperature increment of the $n_{rare} = n_{cr}$ and 300 μm thickness case is, however, strongly reduced and the degradation reaches 50% because of much less appropriate fast electrons for core heating. (see Fig. 6d) If the degradation of less than 10% is acceptable for the fast ignition, ρL of the rarefied plasma must be smaller than 50 n_{cr}·μm. On the other hand, too small ρL plasma cannot absorb the pre-pulse and it hits the cone wall to generate long-scale preformed plasmas. Therefore, we must optimize the film thickness against the pre-pulse intensity and more researches are needed.

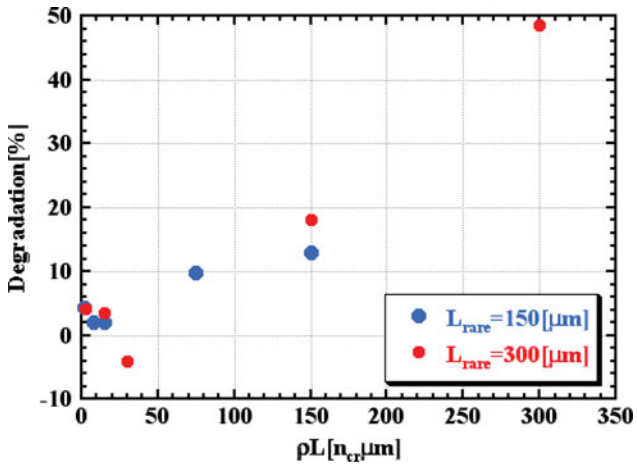

Fig. 8. (Color online) Degradations of electron temperature increment against the case without rarefied plasmas as a function of ρL n_{cr}·μm for both L_{rare} = 150(blue) and 300(red) μm.

4. SUMMARY

We estimated the pre-pulse energy, intensity, and duration to be 130 mJ, 10^{13} W/cm^2, and 1 ns, respectively, by comparing simulation results with experimental observations for planar targets. We simulated the pre-plasma formation inside the cone by the pre-pulse with above parameters and found that the inner space of the cone is filled with preformed plasmas up to 300 μm away from the cone tip. This is also suggested by the wide bright area in X-ray pinhole images away from the cone tip in 2009 experiments. After that, we performed simulations to evaluate preformed plasma effects inside the cone and found that the energy coupling rate from the laser to fast electrons especially suitable for core heating is drastically reduced due to the long-scale preformed plasma inside the cone.

To mitigate the serious problem of preformed plasmas, we proposed to install the thin film that covers the entrance of the cone. This method, however, introduces long rarefied plasmas, which could affect fast electron characteristics produced by the main pulse, around the entrance of the cone. Thus, we investigated effects of long rarefied plasmas on fast electron generation and found that the electron beam intensity

https://doi.org/10.1017/S0263034611000735 Published online by Cambridge University Press

becomes larger than that without rarefied plasmas, but coupling efficiency from the heating laser to the core decreases due to lack of appropriate fast electrons for core heating. If the length of the rarefied plasma is 500 μm (1 mm) and we can accept 10% degradation of the core electron temperature, the thin film must be expanded by irradiation of the pre-pulse so that the density of the remnant plasma becomes less than $0.1n_{cr}$ ($0.05n_{cr}$). Thicker film will introduce the remnant plasma, whose density is higher than the criterion or thinner film can not absorb the pre-pulse enough to disturb the formation of preformed plasmas inside the cone. So we can determine the optimum thickness of the thin film related with these criteria and the pre-pulse intensity. As the remnant plasma of 0.1 μm CH thin film simulated in Section 2.2 can be expected to satisfy the criteria under current pre-pulse conditions, our conclusion supports the pre-pulse suppression method by the CH thin film.

Of course, the laser plasma interactions are simulated by one-dimensional particle-in-cell code in this work, but relativistic self-focusing will play an important role because the heating laser power in FIREX-I is the order of PW and beyond the threshold even if the density of the rarefied plasma is $0.01n_{cr}$. This effect should be treated by multi-dimensional PIC code. Multi-dimensional analyses including laser beam diverging/merging and phase distortion in the rarefied plasma are also needed to clarify our conclusion.

ACKNOWLEDGMENT

This work is partially supported by JSPS grant-in-aid for scientific research (C 22540511).

REFERENCES

Azechi, H. & Firex Project. (2008). The FIREX program on the way to inertial fusion energy. *J. Phys. Conf. Ser.* **112**, 012002.

Cai, H.B., Mima, K., Zhou, W.M., Johzaki, T., Nagatomo, H., Sunahara, A. & Mason, R.J. (2009). Enhancing the number of high-energy electrons deposited to a compressed pellet via double cones in fast ignition. *Phys. Rev. Lett.* **102**, 245001.

Johzaki, T., Nagatomo, H., Sakagami, H., Sentoku, Y., Nakamura, T., Mima, K., Nakao, Y. & Yokota, T. (2006). Core heating analysis of fast ignition targets by integrated simulations. *J. Phys. IV* **133**, 385–389.

Johzaki, T., Sakagami, H., Nagatomo, H. & Mima, K. (2007). Holistic simulation for FIREX project with FI^3. *Laser Part. Beams* **25**, 621–629.

Johzaki, T., Sentoku, Y., Nagatomo, Sakagami, H., Nakao, Y. & Mima, K. (2009). Core heating properties in FIREX-I: Influence of cone tip. *Plasma Phys. Contr. Fusion* **51**, 014002.

Johzaki, T., Nagatomo, H., Sunahara, A., Cai, H.B., Sakagami, H. & Mima, K. (2010). Integrated simulations of core heating in cone-guiding fast ignition FIREX-I. *J. Phys. Conf. Ser.* **244**, 022040.

Johzaki, T., Nagatomo, H., Sunahara, A., Cai, H.B., Sakagami, H., Nakao, Y. & Mima, K. (2011). Pre-plasma effects on core heating and enhancing heating efficiency by extended double cone for FIREX. *Nucl. Fusion* **49**, 073022.

Kemp, A.J., Sentoku, Y. & Tabak, M. (2009). Hot-electron energy coupling in ultraintense laser-matter interaction. *Phys. Rev. E* **79**, 066406.

Kinoshita, K., Zhidkov, A., Hosokai, T., Ohkubo, T. & Uesaka, M. (2004). Propagation of an intense femtosecond laser pulse through a thin foil filter. *App. Phys. Lett.* **84**, 4623–4625.

Kodama, R., Shiraga, H., Shigemori, K., Toyama, Y., Fujioka, S., Azechi, H., Fujita, H., Habara, H., Hall, T., Izawa, Y., Jitsuno, T., Kitagawa, Y., Krushelnick, K.M., Lancaster, K.L., Mima, K., Nagai, K., Nakai, M., Nishimura, H., Norimatsu, T., Norreys, P.A., Sakabe, S., Tanaka, K.A., Youssef, A., Zepf, M. & Yamanaka, T. (2002). Nuclear fusion: Fast heating scalable to laser fusion ignition. *Nat.* **418**, 933–934.

Kondo, K., Maeda, H., Hama, Y., Morita, S., Zoubir, A., Kodama, R., Tanaka, K.A., Kitagawa, Y. & Izawa, Y. (2006). Control of amplified optical parametric fluorescence for hybrid chirped-pulse amplification. *J. Opt. Soc. Am.* **B23**, 231–235.

Mima, K., Sunahara, A., Shiraga, H., Nishimura, H., Azechi, H., Nakamura, T., Johzaki, T., Nagatomo, H., Garcia, C. & Veralde, P. (2010). FIREX project and effects of self-generated electric and magnetic fields on electron-driven fast ignition. *Plasma Phys. Contr. Fusion* **52**, 124047.

Nagatomo, H., Ohnishi, N., Mima, K., Sawada, K., Nishihara, K. & Takabe, H. (2002). Analysis of hydrodynamic instabilities in implosion using high-accuracy integrated implosion code. *Proc. 2nd Int. Conf. on Inertial Fusion Sciences and Applications*, pp. 140–142. Paris: Elsevier.

Nakamura, T., Sakagami, H., Johzaki, T., Nagatomo, H. & Mima, K. (2006). Generation and transport of fast electrons inside cone targets irradiated by intense laser pulses. *Laser Part. Beams* **24**, 5–8.

Nakamura, T., Mima, K., Sakagami, H., Johzaki, T. & Nagatomo, H. (2008). Generation and confinement of high energy by irradiation of ultra-intense short laser pulses onto cone targets. *Laser Part. Beams* **26**, 207–212.

Sakagami, H. & Mima, K. (2002). Fast ignition simulations with collective PIC code. *Proc. 2nd Int. Conf. on Inertial Fusion Sciences and Applications*, pp. 380–383. Paris: Elsevier.

Sakagami, H. & Mima, K. (2004). Interconnection between hydro and PIC codes for fast ignition simulations. *Laser Part. Beams* **22**, 41–44.

Sakagami, H., Johzaki, T., Nagatomo, H. & Mima, K. (2006). Fast ignition integrated interconnecting code project for cone-guided targets. *Laser Part. Beams* **24**, 191–198.

Sakagami, H., Johzaki, T., Nagatomo, H. & Mima, K. (2009). Generation control of fast electron beam by low density foam for FIREX-I. *Nucl. Fusion* **49**, 075026.

Sunahara, A., Sasaki, A. & Nishihara, K. (2008). Two-dimensional radiation hydrodynamic simulation for extreme ultra-violet emission from laser-produced tin plasmas. *J. Phys. Conf. Ser.* **112**, 042048.

Sunahara, A., Johzaki, T., Nagatomo, H., & Mima, K. (2012). Generation of pre-formed plasma and its reduction for fast-ignition. *Laser Part. Beam* doi: 10.1017/S0263034611000723.